A PARAMETRIC STUDY OF THE HYDROELASTIC RESPONSE OF A FLOATING, MAT-TYPE RUNWAY IN REGULAR WAVES

R. Cengiz Ertekin and Jang Whan Kim
Dept. of Ocean Engineering, SOEST, Univ. of Hawaii at Manoa *

June 15, 1998

Abstract:
The linear, Level I Green-Naghdi (GN) theory is developed to study the hydroelastic behavior of a rectangular airport or runway whose draft is "small" and which floats in a near-shore area. The theory uses the linear, shallow-water wave equations of the GN type for the fluid dynamics and the thin-plate theory for the structural dynamics. The governing equations are matched at the juncture boundary and the resulting partial differential equations are solved by the boundary-integral-equation (BIE) method. The method devised here is proven to be very efficient in a parametric study of the hydroelastic response of a mat-type floating runway in regular waves. The main parameter varied in the problem is the stiffness of the mat. The deflections of the mat are calculated for various incoming wave frequencies and heading angles in water of "shallow" depth. The presented results may be used as a guideline to determine the stiffness of a mat-type floating airport at the preliminary design stage.

I- Introduction

Mat-type structures are usually considered as floating runways or airports in relatively shallow water and in sheltered locations. The use of a simple geometry, that of a wall-sided, shallow, rectangular shape as a floating airport is planned, e.g., in Japan (see [1]). Because a floating runway would be very long and wide, it is necessarily quite flexible and can respond in a three-dimensional way to incoming waves. If the response is not confined to the edges of the runway, the taking-off and landing operations of an airplane can severely be affected. Therefore, it is important that we understand the physical mechanism behind the dynamics of such elastic structures.

The hydroelastic response of a floating mat to incoming waves has typically been treated in the past by panel (the Green function) methods and in the frequency domain. In panel methods, the major computational effort is made to solve the fluid problem. Because the length of the incident wave is smaller than the length and, in some cases, even the beam of the mat, the number of panels required for sufficient accuracy is very large. This presents difficulties in using the panel methods as quantitative analysis tools for design.

Recently, a new approach based on the Green-Naghdi (GN) theory is proposed by [2]. The kinematic structure of the fluid motion beneath and outside the plate is simply assumed to follow the linear, Level I GN theory. The velocity fields in the regions with and without the plate are matched using the continuity of mean mass flux and pressure. The new method was devised to study an infinitely-long plate in oblique waves. The results showed good agreement with the available experiment data.

In this study, the work of [2] is extended to a floating mat of finite length by using the linear, Level I GN theory to determine the hydroelastic behavior of a rectangular runway whose draft is "small" and which floats in a near-shore area. Due to lack of space here, the reader is referred to [3] for the full development of the theory and additional results. The theory uses the shallow-water wave equations of the GN type for the fluid dynamics and the thin-plate theory for the structural dynamics. The governing equations are matched at the juncture boundary and the resulting equations are solved by the BIE method in the frequency domain.

The method developed here is very efficient in the parametric study of the hydroelastic response of a mat-type floating runway in regular waves because, unlike in the usual panel methods which require the discretization of the entire mat, we only need to discretize the mat along its edges so that the time-consuming evaluation of surface integrals is replaced by the evaluation of line integrals with much more efficiency. The theory is applied to a mat-type structure with different values of bending stiffness and the deflections of the mat are presented for various incoming wave frequencies and heading angles.

II- Theory

An elastic mat of rectangular plan geometry, with length, L, and beam, B, is considered, see Fig. 1. The mat is

*2540 Dole Street, Holmes Hall 402, Honolulu, HI 96822, USA.

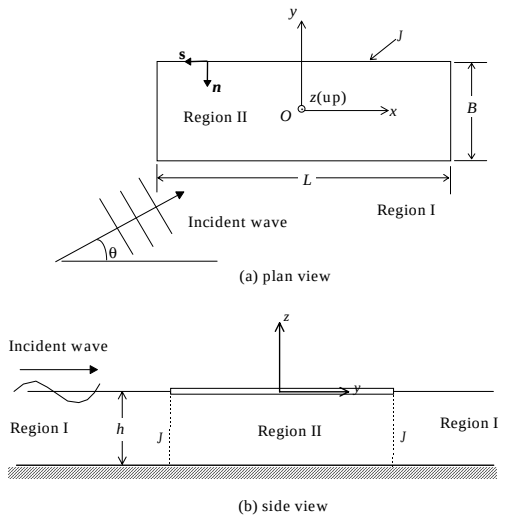

Figure 1: Definition sketch of the problem.

freely floating on an inviscid layer of constant density ρ and depth h, and is under the action of linear shallow-water waves of frequency ω and direction θ. Two regions which describe the fluid region (I) and the fluid-plate region (II) are considered, and these regions are separated by the juncture boundary J.

The rectangular mat is assumed to have a uniform mass distribution, m, and flexural rigidity (per unit width) $D = EI/B$, where E is Young's modulus and I is the moment of inertia of plate cross section. The vertical displacement, ζ, of the mat is assumed to be governed by the plate theory:

$$m\frac{\partial^2\zeta}{\partial t^2} + D\Delta^2\zeta = p_f, \tag{1}$$

where $p_f = p_f(x,y,t)$ is the pressure on the bottom of the plate and $\Delta = \partial^2/\partial x^2 + \partial^2/\partial y^2$ is the two-dimensional Laplacian on the horizontal plane. Since the plate is freely floating, the bending moment and the shear force should vanish at the edges of the plate:

$$\frac{\partial^2\zeta}{\partial n^2} + \nu\frac{\partial^2\zeta}{\partial s^2} = 0, \qquad \frac{\partial^3\zeta}{\partial n^3} + (2-\nu)\frac{\partial^3\zeta}{\partial n\partial s^2} = 0, \tag{2}$$

where n and s denote the normal and tangential directions as seen in Fig. 1, and ν is Poisson's ratio.

We assume that the linear, Level I GN equations govern the time-harmonic fluid motion. The spatial part of the top surface deformation $\zeta = \Re\left\{\zeta'(x,y)e^{-i\omega t}\right\}$ in the fluid and fluid-plate regions is given by a complex function:

$$\zeta' = \frac{h}{i\omega}\Delta\psi, \quad i = \sqrt{-1}, \tag{3}$$

where $\psi(x,y)$ is the mean velocity potential, i.e., $\mathbf{V}(x,y,t) = \Re\left\{\nabla\psi e^{-i\omega t}\right\}$ is the horizontal-velocity vector. The vertical velocity in the theory is given by $w(x,y,t) = \Re\left\{-i\omega\zeta' e^{-i\omega t}(z+h)/h\right\}$. Note that, in this formulation, we implicitly assumed that the effect of the draft of the mat on the flow is negligible.

If we couple the conservation of momentum statement of the GN equations (see [3]) with Eq. (1), we can obtain the governing equation in Region II:

$$D\Delta^3\psi_{II} + \rho g\Delta\psi_{II} - \left(m + \frac{\rho h}{3}\right)\omega^2\Delta\psi_{II} + \frac{\rho\omega^2}{h}\psi_{II} = 0. \tag{4}$$

The governing equation in Region I is given by:

$$\Delta\psi_I + k_0^2\psi_I = 0, \tag{5}$$

where k_0 is the wave number of incoming waves, and we have set the atmospheric pressure to zero.

The solutions of Eqs. (4) and (5) must be coupled through the matching conditions of the mean mass flux and pressure on J:

$$\psi_I = \psi_{II}, \qquad \frac{\partial\psi_I}{\partial n} = \frac{\partial\psi_{II}}{\partial n}. \tag{6}$$

It can be shown, from Eq. (4), that the solution in Region II can be written as $\psi_{II} = \psi_1 + \psi_2 + \psi_3$, and each ψ_j is governed by

$$\Delta\psi_j + {k_j}^2\psi_j = 0, \quad j = 1,2,3 \text{ (no sum on j)}, \tag{7}$$

where k_j's are the roots of the characteristic equation of (4) and $\Re\{k_j\}$ and $\Im\{k_j\} \geq 0$. Physically, these roots are related to the progressive and evanescent (decaying) modes of the hydroelastic waves on the mat.

On the other hand, the solution in Region I can be decomposed as the sum of the incoming and disturbance potentials, i.e., $\psi_I = \psi_0 + \psi_4$. The spatial part, ψ_0, of the incoming potential is given by

$$\psi_0 = -\frac{i\omega A}{k_0^2 h}e^{i(k_x x + k_y y)}, \tag{8}$$

where $k_x = k_0\cos\theta$ and $k_y = k_0\sin\theta$ are the components of the wavenumber vector in the x and y directions, respectively, and A is the wave amplitude. The unknown disturbance potential ψ_4 must also satisfy the radiation condition. From Eq. (5), the wavenumber of ψ_4 is $k_4 = k_0$.

The solution of Helmholtz's equation, Eq. (5) or (7) is called Weber's solution (see e.g., [4]), and is given by the following integral equation to be evaluated along the projection of the juncture boundary onto the mat:

$$\alpha\psi_j(x,y) = -\int_J \left\{\psi_j(\xi,\eta)\frac{\partial G_j}{\partial n} - G_j\frac{\partial\psi_j(\xi,\eta)}{\partial n}\right\} dl_{\xi\eta}, \tag{9}$$

where $\alpha = \pi$ if $j = 1,2,3$ and $\alpha = -\pi$ if $j = 4$, (x,y) is the field point, (ξ,η) is the source point, $l_{\xi\eta}$ is the

arc-length variable along J, and $G_j(x,y;\xi,\eta)$ are the Green functions given by $G_j = \pi H_0^{(1)}(k_j r)/2i$, where $r = \left\{(x-\xi)^2 + (y-\eta)^2\right\}^{1/2}$ is the distance between the field point and the source point, and $H_0^{(1)}$ is the Hankel function of zeroth order.

The projection of the juncture boundary J onto the mat is now discretized by N_e segments on which ψ_j and $\partial\psi_j/\partial n$ are assumed to be piecewise constant functions. The discrete values of these functions can be determined from algebraic equations obtained by discretizing Eq. (2) by the finite-difference method and Eqs. (6) and (9) by collocation at the center of each segment. Once the potential and its derivatives are obtained along the edges of the mat, an integral relation, Eq. (9) with $\alpha = 2\pi$, is used to find the potential anywhere on the plate. The deflections of the mat and the free-surface elevation follow from Eq. (3) in a straightforward manner.

III- **Application**

Based on the BIE method described above, a parametric study is conducted on Japan's MEGA Float project whose specifications are given as $D = 7.8 \times 10^9$N-m $L = 300$m, $B = 60$m, $h = 8$m, (see [5]). Poisson's ratio, ν, is assumed to be 0.3 here. Along the edge of the plate, the amplitude of deflection and the relative wave elevation, which can indicate the runup or slamming, are compared for various values of the stiffness of the plate and the ratio of the plate length to wave length. Along the center of the plate, $y = 0$, the maximum amplitude of the deflection and slope, which are important in the landing and take-off operations of the runway, are comparatively studied. Part of the results for three different values of the bending stiffness, $D_1 = 7.8\times10^8$, $D_2 = 7.8\times10^9$ and $D_3 = 7.8 \times 10^{10}$N-m, and for two different values of the plate to wave length ratio, $L/\lambda = 2$ and 3, are presented here; the corresponding wave periods are 16.9s and 11.3s, respectively.

Fig. 2 shows the amplitude of deflection (per unit wave amplitude) at the lower-left corner ($x = -L/2$, $y = -B/2$) and upper-right corner of the plate ($x = L/2$, $y = B/2$) as functions of the wave angle. It is seen that the deflections at the lower-left corner is not so sensitive to the wave angle, whereas the deflections at the upper-right corner varies considerably with respect to the wave angle. For the original MEGA Float model, for which $D = D_2 = 7.8\times10^9$N-m, the maximum deflections occur at $\theta = 55^o$ and 65^o in Fig. 2(a) and (b), respectively. In other words, as the plate becomes stiffer and/or the wave length becomes shorter, the maximum deflections occur at larger values of θ.

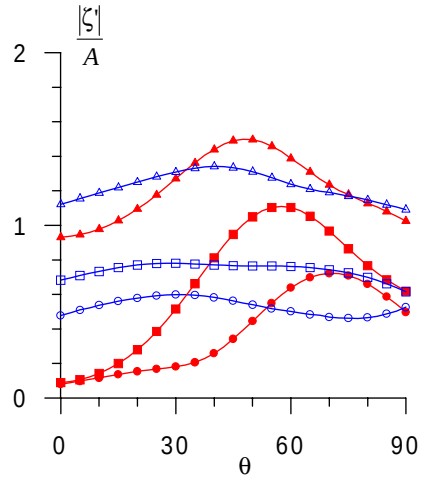

(a) $L/\lambda = 2$

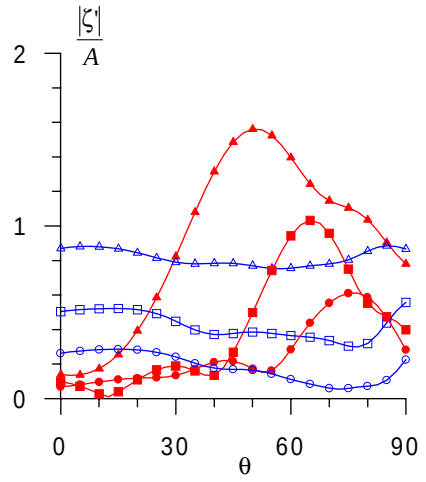

(b) $L/\lambda = 3$

Figure 2: Deflection amplitude at lower-left corner: D_1, D_2, D_3; and at upper-right corner: D_1, D_2, D_3

In Fig. 3, the maximum amplitudes of the deflection and slope along the center are shown. The maximum values are obtained in the region $|x| < L/4$, which is the region of more importance during the landing or take-off of an aircraft. In most cases, it is seen that the deflection and slope decrease as the stiffness of the plate increases or wave length decreases. But when the plate is more flexible, larger values of slope are observed in the shorter wave case, $L/\lambda = 3$.

As a more realistic model for a runway, the model used by [6] is also considered here. The main particulars of the mat are: $D = 3.77 \times 10^{13}$N-m, $\nu = 0.3, L = 5000$m, $B = 1000$m, $h = 50$m. The same model, but with an infinite length, has been used in a 2-D analysis

in [2]. In Fig. 4, the contour plots of the deflection of the runway and wave elevation are shown for $L/\lambda = 10$ and 20. The corresponding wave periods are 22.6s and 11.3s, respectively. The contour level of 1.0 equals the wave amplitude in these figures. When $\theta = 0^{\mathrm{o}}$, the deflection is significant only at the wave side and decreases along the length of the runway. At $\theta = 30^{\mathrm{o}}$, waves are barely transmitted when $L/\lambda = 20$, which is expected since θ is less than the critical angle 52.5^{o} for the given wave length (see [2], for the critical angle defined for an infinitely-wide plate). When $L/\lambda = 10$, the critical angle is 29.6^{o} and, as a result, the waves can be transmitted when $\theta = 30^{\mathrm{o}}$. However, these observations are qualitative because the mat width here is finite.

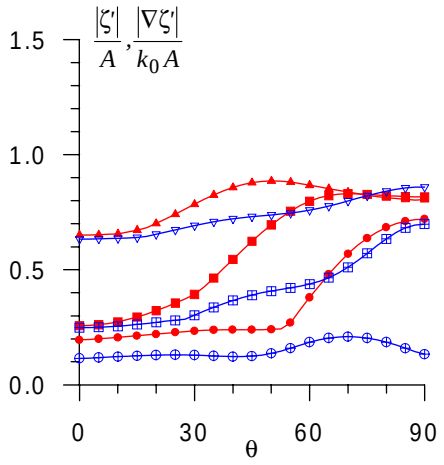

(a) $L/\lambda = 2$

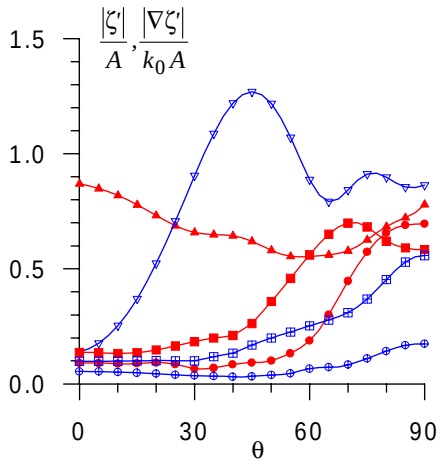

(b) $L/\lambda = 3$

Figure 3: Maximum deflection and slope at center.
Deflection: D_1, D_2, D_3;
Slope: D_1, D_2, D_3

In the analysis of an infinitely-long plate, it has been shown in [2] that the deflection along the center can be large, and waves are totally transmitted when the wave angle is close to the critical angle and the transverse length of the hydroelastic wave on the plate is an even integer times of the width of the plate. This phenomenon is verified using the present numerical method in Fig. 5. The length of the plate is increased by 4 times and other dimensions are left the same as in Fig. 4. The wave angle of 53.4^{o} is considered because, in this case, the transverse length of the hydroelastic wave on the plate is twice that of the width of the plate. Little transmission is observed near the lower-left corner of the plate, as indicated by the checker-board pattern at the wave side. However, the amplitude of the transmitted waves increases as x increases and the amplitude of the deflection along the center of the plate approaches $1.2A$, as also predicted by the 2-D theory of [2]. Also note that the wave amplitude near the right-side edge of the plate in the down-wave region is very high; it is about four times of the incident-wave amplitude.

Acknowledgment: The material is based upon work supported by the U.S. National Science Foundation, Grant No. BES-9532037, managed by Dr. Norman Caplan, and by the U.S. Office of Naval Research's MOB Program, through Float Inc., San Diego, CA. SOEST Contribution No. 4648.

References

[1] Yoshiyasu Watanabe. *Ed., Proc. Int. Workshop on Very Large Floating Structures, VLFS '96, Hayama.* Sip Research Institute, Japan, 1996.

[2] J. W. Kim and R. C. Ertekin. Deformations of an infinitely-long, elastic plate floating in oblique waves: Linear Green-Naghdi theory. *Submitted to J. Fluid Mech.*, 1998.

[3] R. C. Ertekin and J. W. Kim. Hydroelastic response of a floating mat-type structure in oblique, shallow-water waves. *Submitted to J. Marine Science and Technology*, 1998.

[4] V. W. Harms. Diffraction of water waves by isolated structures. *J. Waterway, Port, Coastal and Ocean Div., ASCE*, 105(WW2), pp. 131–147, 1979.

[5] K. Yago and Endo H. Model experiment and numerical calculation of the hydroelastic behavior of matlike vlfs. In *Proc. Int. Workshop on Very Large Floating Structures, Japan*, pp. 209–216, 1996.

[6] M. Kashiwagi. A B-spline Galerkin method for computing hydroelastic behavior of a very large floating structure. In *Proc. Int. Workshop on Very Large Floating Structures, Japan*, pp. 149–156, 1996.

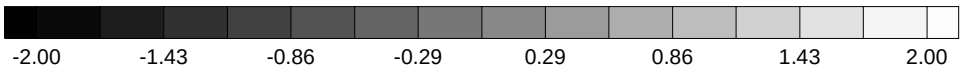

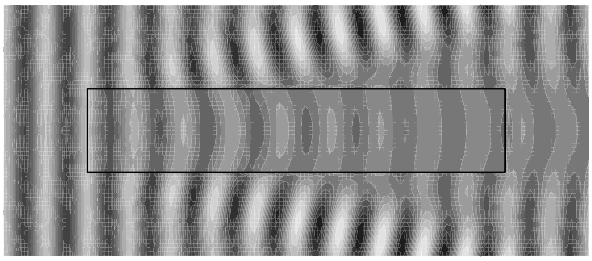

(a) $L/\lambda = 10, \theta = 0^{\mathrm{o}}$

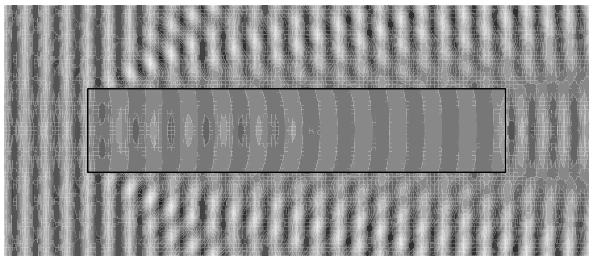

(b) $L/\lambda = 20,\ \theta = 0^{\mathrm{o}}$

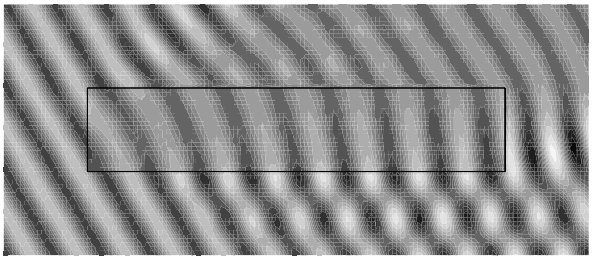

(c) $L/\lambda = 10, \theta = 30^{\mathrm{o}}$

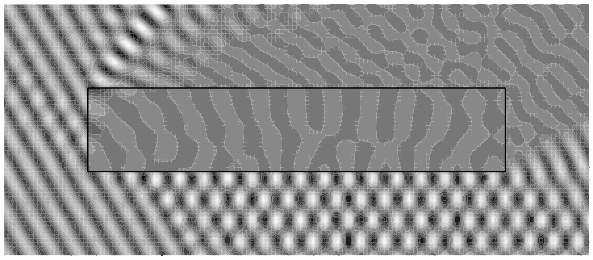

(d) $L/\lambda = 20,\ \theta = 30^{\mathrm{o}}$

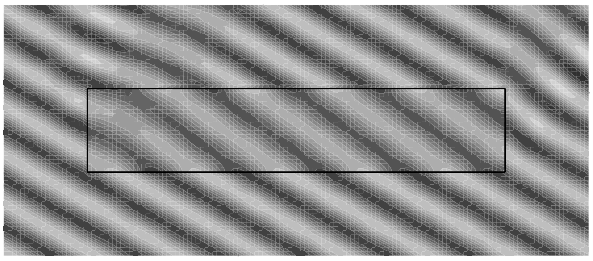

(e) $L/\lambda = 10, \theta = 60^{\mathrm{o}}$

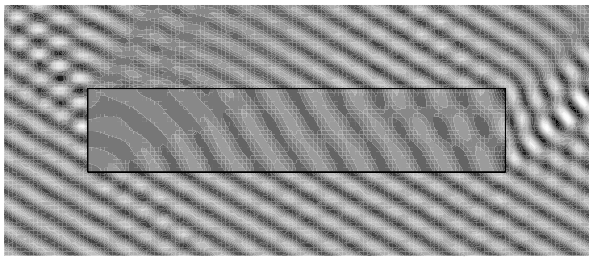

(f) $L/\lambda = 20,\ \theta = 60^{\mathrm{o}}$

Figure 4: Contour plots of $\Re\{\zeta'\}/A$: $L = 5\,\mathrm{km}, B = 1\,\mathrm{km},\ h = 50\,\mathrm{m}$

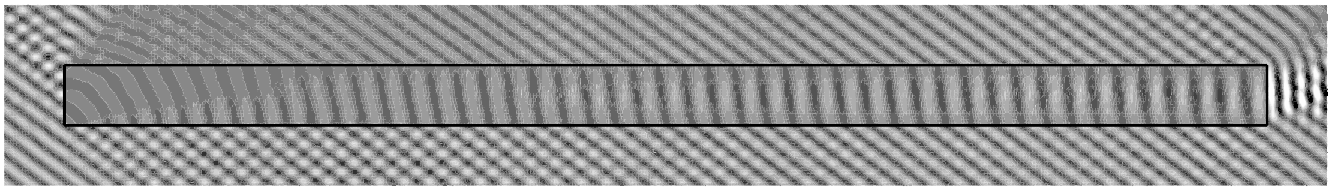

Figure 5: Contour plots of $\Re\{\zeta'\}/A$: $L/\lambda = 80,\ \theta = 53.4^{\mathrm{o}}$; $L = 20\,\mathrm{km},\ B = 1\,\mathrm{km},\ h = 50\,\mathrm{m}$